HHS Public Access

Author manuscript

Dev Biol. Author manuscript; available in PMC 2017 December 01.

Published in final edited form as:

Dev Biol. 2017 December 01; 432(1): 125–139. doi:10.1016/j.ydbio.2017.09.023.

Intraflagellar Transporter Protein (IFT27), an IFT25 binding partner, Is Essential For Male Fertility and Spermiogenesis In Mice

Yong Zhang[1,2], **Hong Liu**[2,3], **Wei Li**[2], **Zhengang Zhang**[2,4], **Xuejun Shang**[5], **David Zhang**[6], **Yuhong Li**[2,7], **Shiyang Zhang**[2,3], **Junpin Liu**[2,8], **Rex A Hess**[9], **Gregory J Pazour**[10], and **Zhibing Zhang**[2,*]

[1]Department of Dermatology, Tongji Hospital affiliated to Tongji Medical College, Huazhong University of Science and Technology, Wuhan China, 430030

[2]Department of Obstetrics & Gynecology, Virginia Commonwealth University, Richmond, VA, 23298

[3]School of Public Health, Wuhan University of Science and Technology, Wuhan, Hubei, 430060

[4]Department of Gastroenterology, Tongji Hospital Affiliated to Tongji Medical College, Huazhong University of Science and Technology, Wuhan, Hubei, 430030

[5]Department of Andrology, Jinling Hospital, Nanjing University, School of Medicine, Nanjing, China

[6]Godwin High School, 2101 Pump Rd Richmond, VA 23238

[7]Department of Pathology, School of Medicine, Wuhan University of Science and Technology, Wuhan, Hubei, 430060

[8]Wuhan Hospital for the Prevention and Treatment of Occupational Diseases, Wuhan, 430000, Hubei, China

[9]Comparative Biosciences, College of Veterinary Medicine, University of Illinois, 2001 S. Lincoln, Urbana, IL 61802-6199

[10]Program in Molecular Medicine, University of Massachusetts Medical School, Worcester, MA 01605

Abstract

Intraflagellar transport (IFT) is an evolutionarily conserved mechanism essential for the assembly and maintenance of most eukaryotic cilia and flagella. In mice, mutations in IFT proteins have been shown to cause several ciliopathies including retinal degeneration, polycystic kidney disease, and hearing loss. However, little is known about its role in the formation of the sperm tail, which

*Address correspondence to: Zhibing Zhang, MD, PhD, Associate Professor, Department of Obstetrics/Gynecology, Virginia Commonwealth University, 1101 E Marshall Street Richmond, VA, 23298. zhibing.zhang@vcuhealth.org.

has the longest flagella of mammalian cells. IFT27 is a component of IFT-B complex and binds to IFT25 directly. In mice, IFT27 is highly expressed in the testis. To investigate the role of IFT27 in male germ cells, the floxed *Ift27* mice were bred with *Stra8-iCre* mice so that the *Ift27* gene was disrupted in spermatocytes/spermatids. The *Ift27:Stra8-iCre* mutant mice did not show any gross abnormalities, and all of the mutant mice survive to adulthood. There was no difference between testis weight/body weight between controls and mutant mice. All adult homozygous mutant males examined were completely infertile. Histological examination of the testes revealed abnormally developed germ cells during the spermiogenesis phase. The epididymis contained round bodies of cytoplasm. Sperm number was significantly reduced compared to the controls and only about 2% of them remained significantly reduced motility. Examination of epididymal sperm by light microscopy and SEM revealed multiple morphological abnormalities including round heads, short and bent tails, abnormal thickness of sperm tails in some areas, and swollen tail tips in some sperm. TEM examination of epididymal sperm showed that most sperm lost the “9+2” axoneme structure, and the mitochondria sheath, fibrous sheath, and outer dense fibers were also disorganized. Some sperm flagella also lost cell membrane. Levels of IFT25 and IFT81 were significantly reduced in the testis of the conditional *Ift27* knockout mice, and levels of IFT20, IFT74, and IFT140 were not changed. Sperm lipid rafts, which were disrupted in the conditional *Ift25* knockout mice, appeared to be normal in the conditional *Ift27* knockout mice. Our findings suggest that like IFT25, IFT27, even though not required to ciliogenesis in somatic cells, is essential for sperm flagella formation, sperm function, and male fertility in mice. IFT25 and IFT27 control sperm formation/function through many common mechanisms, but IFT25 has additional roles beyond IFT27.

Keywords

Male infertility; intraflagellar transport; sperm flagella formation; ciliogenesis; germ cells

Introduction

Intraflagellar transport (IFT) is the process operating between the ciliary/flagellar membrane and the microtubular axoneme of motile and primary cilia (Ishikawa and Marshall, 2017; Mourao et al., 2016; Prevo et al., 2017). IFT particles, composed of complexes A and B, carry flagellar cargo proteins to their assembly site at the flagellar tip by driven by kinesin (Scholey, 2013), and turnover products from the tip back to the cytoplasm by cytoplasmic dynein (Hou and Witman, 2015). About twenty-two *Ift* genes haven been identified: six belong to complex A and the rest belong to complex B. Even though originally discovered in *Chlamydomonas*, IFT orthologues were present in mammals. Defects in the IFT components have been shown to cause a spectrum of diseases, ranging from developmental defects to obesity, diabetes, and cancer. Many of these diseases, or ciliopathies, manifest as genetic syndromes, such as Joubert syndrome, Bardet-Biedel (BBS), Meckel-Gruber (MKS), and Nephronophthisis (NPHP)(Barker et al, 2014; Nozaki et al., 2017; Srivastava and Sayer, 2014; Su et al, 2014; Suspitsin and Imyanitov, 2016).

IFT27 was originally reported to be a subunit of IFT complex B of *Chlamydomonas*, where it forms a core complex together with IFT88, IFT81, IFT74, IFT72, IFT52, and IFT46

(Lucker et al, 2005). The gene was subsequently cloned by MALDI-TOF sequencing of the protein recovered from the SDS-PAGE gel. *Chlamydomonas* IFT27 contains all five Ras-GTPase consensus sequences that are essential for GDP/GTP binding and GTPase activity. It is not only present in flagella, but also in the cell body, principally around the basal bodies. GFP-labeled IFT27 undergoes typical IFT bidirectional transport in the *Chlamydomonas* flagella. In *Chlamydomonas*, IFT27 conducts dual functions. In addition to its role in flagellar assembly, during cell division, IFT27 re-localized from the flagella and basal bodies to the cleavage furrow, and it is associated with membrane vesicles in this region. In addition, IFT27 is instrumental in maintaining the stability of both IFT complexes (Qin et al, 2007; Wood et al, 2012). In *Trypanosoma brucei*, IFT27 is involved in anterograde and retrograde intraflagellar transport and is required for cell growth and flagellum formation in (Huet et al., 2014).

IFT27 directly interacts with IFT25, and these two proteins likely form a subcomplex *in vivo*. In flagella, the majority of IFT27 and IFT25 are co-sedimented with other complex B subunits. In contrast, in cell body, only a fraction of IFT25 and IFT27 is integrated into the preassembled complex B (Wang et al, 2009). The structure base of *Chlamydomonas* IFT25/IFT27 interaction was studied. IFT25 and IFT27 interact via a conserved interface. IFT27 displays the fold of Rab-like small guanosine triphosphate hydrolases (GTPases). A patch of conserved surface residues contributed by both IFT25 and IFT27 is found adjacent to the GTP-binding site and could mediate the binding to other IFT proteins (Bhogaraju et al., 2011).

Even though no orthologue of IFT27 was identified in the genomes of *C. elegans* or *Drosophila* (Keady et al, 2012; Lechtreck et al, 2009), IFT27 orthologue is present in mammals and zebrafish. It has been reported that mutations of human *IFT27* gene associate with several genetic disorders, including bipolar disorder and BBS (Aldahmesh et al, 2014; Forsythe and Beales, 1993; Nissen et al, 2012), and it is also named as BBS 19, a member of BBS genes (Forsythe and Beales, 1993). Zebrafish embryos co-injected with the established morpholino oligo against *Ift27* mRNA display typical ciliopathy phenotypes (Aldahmesh et al, 2014). The role of IFT27 was further investigated in mice. *Ift27* null mutants display multiple developmental defects, including abnormal facial structure, skull palate development, nasal cavities, and structural heart and lung diseases, and these defects result in animal death at birth (Eguether et al, 2014). Surprisingly, cilia formation in the MEFs, lung and cortical collecting ducts are not affected in the *Ift27* mutant mice. However, *Ift27* mutants have Hedgehog signaling defects. The accumulated Smoothened, GPR161 and Lztfl1 suggested that IFT27 controls the exit of these proteins from cilia (Eguether et al, 2014). IFT27 likely works through ARL6 as IFT27 directly interacts with and stabilizes nucleotide-free ARL6. A possible mechanism has IFT27 activating ARL6 to promote BBSome assembly within the cilium to drive removal of signaling molecules like smoothened and GPR161 (Liew et al., 2014).

IFT27 also plays a role in hair follicle morphogenesis. Normal hair follicle morphogenesis depends on normal hedgehog (Hh) signaling within the primary cilia, disrupting ciliogenesis results in hair follicle morphogenesis defects due to attenuated Hh signaling (Lehman et al., 2009). Hair follicle morphogenesis of *Ift27*-null mice was severely impaired; the Hh

signaling pathway was attenuated in *Ift27* mutants, which was in association with abnormal ciliary trafficking of SMO and GLI2, and impaired processing of Gli transcription factors; however, formation of the ciliary axoneme was unaffected (Yang et al, 2015).

Even though the important functions of IFT components in cilia have been shown in other organisms and somatic cells in mice and the fact that global disruption of IFT usually result in embryonic death (Marszalek et al, 1999; Nonaka et al, 1998), the role of IFT in male germ cells, which have the longest motile cilia, remains largely unknown. It has been reported that the surviving hypomorphic mutant *Ift88* (Tg737Rpw) mice are completely sterile due to the failure of formation of functional sperm flagella (San Agustin et al., 2015). Using conditional knockout strategy, our laboratory disrupted mouse *Ift20* and *Ift25* genes in male germ cells, and discovered that both were essential for male fertility, spermiogenesis, and sperm flagella formation (Liu et al., 2017; Zhang et al., 2016). Using the same strategy, we disrupted *Ift27* gene in mouse germ cells, and discovered that the gene is essential for male fertility and spermatogenesis. Surprisingly, unlike in some somatic cells where IFT27 is dispensable for ciliogenesis, IFT27 is required for sperm flagellar formation, which is similar to IFT25. Our studies demonstrated that IFT27 plays different roles in male germ cells and somatic cells.

Materials and Methods

Ethics Statement

All animal studies were approved by Virginia Commonwealth University Institutional Animal Care and Use Program Advisory Committee (Protocol number: AD10000167).

Genetically Altered Mice

Stra8-iCre mice were purchased from Jackson Laboratory (Stock No: 008208). Transgenic mouse line *Stra8-cre* expresses improved Cre recombinase under the control of a 1.4 Kb promoter region of the germ cell-specific stimulated by retinoic acid gene 8 (*Stra8*) (Sadate-Ngatchou et al., 2008). $Ift27^{flox/flox}$ mice were generated by Dr. Gregory J. Pazour, University of Massachusetts Medical School, and exons 3–5 were floxed in the $Ift27^{flox/flox}$ mice (Eguether et al, 2014). To generate germ cell specific *Ift27* knockout mice, we followed the same breeding strategy as to generate germ cell specific *Ift20* and *Ift25* knockout mice (Liu et al, 2017; Zhang et al, 2016). Briefly, three to four-month old *Stra8-cre* males were crossed with three to four-month old $Ift25^{flox/flox}$ females to obtain *Stra8-iCre;* $Ift25^{flox/+}$ mice. The three to four-month old *Stra8-iCre;* $Ift25^{flox/+}$ males were crossed back with three- to four-month old $Ift25^{flox/flox}$ females again, and the *Stra8-iCre;* $Ift25^{flox/flox}$ were considered to be the homozygous knockout mice (KO), and *Stra8-iCre;* $Ift2^{flox/+}$ mice were used as the controls. Mice were genotyped by PCR using multiplex PCR mix (Bioline, Cat No BIO25043). The presence of the *Stra8-iCre* allele was evaluated as described in (Sadate-Ngatchou et al, 2008), and *Ift27* genotypes were determined as described previously (Eguether et al, 2014).

Real-time PCR

Total tissue RNA was isolated using TRIZOL reagent (QIAGEN), and cDNA was synthesized using a first strand cDNA SensiFASTTM cDNA Synthesis Kit (BIOLINE). To compare *Ift27* mRNA expression levels in different mouse tissues, qPCR was conducted using the following primer pair designed with GeneScript tools: Forward: 5'-GTGAAGCTAGCTGCCAAATG-3', and reverse: 5'-CACTCCAGTTGTCAGGGTGT-3'. Mouse *Gapdf* was used to normalize the expression level.

Western Blot Analysis

Testes from 3–4 months old conditional *Ift27* KO and control mice were pulverized on ice in lysis buffer (50 mM Tris-HCl [pH8.0], 170 mM NaCl, 5 mM ethylenediaminetetra-acetic acid, 1 mM dithiothreitol, and protease inhibitors [Complete mini; Roche Diagnostics GmbH]) containing either 1% NP-40, 0.5% sodium deoxycholate, and 0.05% SDS. After centrifuge at 1200 rpm for 10 minutes, the supernatants were collected, and protein concentrations were measured by Lowry assay. Proteins were denatured and separated under denaturing conditions by SDS-PAGE and transferred to polyvinylidene fluoride membrane. Nonspecific sites were blocked with 5% nonfat dry milk in PBST for 1 hr at room temperature, and the membranes were incubated overnight with the indicated primary antibodies (IFT25: 1:2000, Cat No: 15732-1-AP, ProteinTech; IFT74: 1:1000, Cat No: AAS27620e, from ANTIBODY VERIFY; IFT81: 1:1000, Cat No: 11744-1-AP, ProteinTech; β-actin: 1:2000, Cat No: 4967S, Cell Signaling; Antibodies against IFT20, IFT27 and IFT140 (1:2000) were from Dr. Pazour's laboratory (Jonassen et al, 2012; Keady et al, 2012; Pazour et al., 2002)) followed by incubation with the secondary antibodies conjugated with horseradish peroxidase (Amersham). The bound antibodies were detected with Super Signal Chemiluminescent Substrate (Pierce, Rockford, IL, USA).

Fertility Test

Six-week old or 3–4 months old conditional *Ift27* KO and the control males were paired with adult wild-type females (3–4 months old) to determine fertility. Mating cages typically consisted of one male and one female. The females were checked for the presence of vaginal plugs and pregnancy. Breeding tests for each pair lasted for at least three months. The progeny were collected and fertility rate was counted.

Histology on Tissue Sections

Testes and epididymides of adult mouse were dissected and fixed in 4% formaldehyde solution in PBS, paraffin-embedded, and sectioned into 5 μ m slides. Hematoxylan and Eosin staining was carried out using standard procedures. Histology was examined using a BX51 Olympus microscope (Olympus Corp., Melville, NY, Center Valley, PA), and photographs were taken with the ProgRes C14 camera (Jenoptik Laser, Germany).

Transmission Electron Microscopy (TEM)

Mouse testes and epididymal sperm were fixed in 3 % glutaraldehyde/1 % paraformaldehyde/0.1 M sodium cacodylate, pH 7.4 at 4 °C overnight. The samples were rinsed twice with 0.1M sodium cacodylate guffer and fixed again with 2% osmium

tetroxide/1% potassium ferrocyanide in 0.1M sodium cacodylate buffer at room temperature for 1 hour, rinsed three times with 0.1M sodium cacodylate buffer, dehydrated in 50%, 70%, 80%, 95% ethanol at 4°C and then with 100% ethanol at room temperature. The samples were then treated with propylene oxide three times, followed by incubation with a 1:1 mix of propylene oxide and EMbed 812 resin overnight then pure EMbed 812 resin from 8 hours to overnight with rotation. The samples were then embedded in fresh resin (Embed Resin - Electron Microscopy Sciences, Hatfield, PA). The sections (60 nm sections) were cut with the Leica EM UC6i Ultramicrotome and stained with uranyl acetate and Reynold's lead citrate. Imaged were taken with the JEOL JEM-1230 TEM (or JEOL JEM-1400) using a Gatan Orius SC1000 camera (McDonald, 1984). Two control and two IFT27 KO mice were analyzed. For both sperm and testis samples, total thirty images from the control mice and eighty images from the knockout mice were randomly taken from these mice, and three sections were analyzed from each mouse.

Scanning Electron Microscopy (SEM)

Mouse epididymal sperm were collected and fixed in the same fixative solution as TEM. The samples were processed and images were taken with a Zeiss EVO 50 XVP SEM at Microscopy Facility, Department of Anatomy and Neurobiology, Virginia Commonwealth University.

Spermatozoa Counting

Sperm cells were collected from cauda epididymides in PBS, and fixed in 2% formaldehyde for ten minutes at room temperature. After washing with PBS, sperm were suspended into PBS again and counted using a hemocytometer chamber under a light microscope, and sperm number was calculated by standard method as we used previously (Zhang et al, 2009).

Sperm Motility Assay

Spermatozoa were collected from the cauda epididymides and placed in warm PBS. Sperm motility was evaluated under non-capacitation condition in PBS using a Nikon TE200E inverted microscope on a pre-warmed slide with SANYO color CCD, Hi-resolution camera (VCC-3972) and Pinnacle Studio HD (Ver. 14.0) software. For each sperm sample, eight fields were randomly selected for analysis. Individual spermatozoa were tracked using the NIH ImageJ (NIH, Bethesda, MD, USA) and the plugin MTrackJ. Sperm motility was calculated as curvilinear velocity (VCL), which is equivalent to the curvilinear distance (DCL) that is travelled by each individual spermatozoa in one second (VCL=DCL/t).

Isolation of spermatogenic cells and immunofluorescence (if) analysis

Testes from adult mice were dissected in a petri dish with 5 mL DMEM containing 0.5 mg/mL collagenase IV and 1.0 μg/mL DNAse I (Sigma-Aldrich), and was incubated for 30 min at 32°C with gentle stirring, released spermatogenic cells were pelleted by centrifugation (5 min at 1000 rpm, 4°C). After washing with PBS, the cells were fixed with 5 ml of 4% paraformaldehyde (PFA) containing 0.1 M sucrose at room temperature. The dispersed, mixed testicular cells were washed three times with PBS. Afterwards, the cells were re-suspended in 2 ml of warm PBS and 50 μl of cell suspension was loaded to the slide

and allowed to air-dry. Cells were permeabilized with 0.1% Triton X-100 (Sigma-Aldrich) for 5 min at 37°C, washed with PBS three times, and blocked with 10 % goat serum in PBS for 1 hr. Then cells were washed three times with PBS and incubated overnight with an anti-IFT27 antibody (1:100, from Dr. Pazour's laboratory) (Eguether et al, 2014). After extensive wash with PBS, the cells were incubated with Cy3-conjugated anti-rabbit IgG secondary antibody for 1 hr. The slides were washed with PBS and mounted in VectaMount with DAPI (Vector Labs. Burlin-game, CA) and sealed with nail polish. Images were captured by confocal laser-scanning microscopy as before.

Immunofluorescence (IF) analysis on tissue sections

Fresh testis, heart and muscle from an adult wild-type mouse were fixed with 4% paraformaldehyde in 0.1 M PBS (pH 7.4), and 5 μm paraffin sections were made. For the immunofluorescence, the sections were incubated with the indicated primary antibodies (IFT27 antibody was the same as used above; anti-acetylated tubulin antibody was from Sigma, Cat #: T6793) at 4°C overnight. Slides were washed with PBS and incubated for 1 hour at room temperature with Alexa 488-conjugated anti-mouse IgG secondary antibody (1:500; Jackson ImmunoResearch Laboratories) or Cy3-conjugated anti-rabbit IgG secondary antibody (1:5000; Jackson ImmunoResearch Laboratories). Following secondary antibody incubation, the slides were washed again three times in PBS, mounted using VectaMount with 4′, 6-diamidino-2-phenylindole (DAPI) (Vector Laboratories, Burlingame, CA), and sealed with a cover slip. Images were captured by confocal laser-scanning microscopy (Zeiss LSM 700).

Sperm Lipid Raft Determination

Sperm were collected from cauda epididymis of 3–4 months old control, conditional *Ift25* KO and *Ift27* KO mice, and then incubated for 30 min with 5μg/ml FITC-labeled Cholera Toxin B subunit (C1655, Sigma, St. Louis, MO 63178) (Watanabe and Kondoh, 2011). The stained sperm were rinsed twice in PBS, and fixed in 4% PFA. After washing 3 times again with PBA, the sperm were seeded onto slides and mounted in VectaMount with DAPI (Vector Labs. Burlin-game, CA) and sealed with nail polish. Images were captured with a Nikon N-SIM Structured Illumination ("Super-Resolution") Microscope at Microscopy Facility, Department of Anatomy and Neurobiology, Virginia Commonwealth University.

Statistical Analysis

ANOVA test was used to determine statistical difference, the 2-tailed student's *t*-test was used for comparison of frequencies. Significance is defined as $P < 0.05$.

Results

Mouse *Ift27* mRNA and protein expression *in vivo*

To examine *Ift27* mRNA expression *in vivo*, RT-PCR was conducted using cDNAs from multiple mouse tissues. It was found that strong signal was amplified only from mouse testis; very weak signals were also present in several other tissues (Fig. 1A). To compare *Ift27* mRNA abundance in these tissues, quantitative PCR was conducted. Consistently, mouse testis has the highest expression level (Fig. 1B).

IFT27 protein expression was examined by Western blot analysis. We first analyzed IFT27 protein expression in various mouse tissues, including heart, brain, lung, liver, kidney, spleen and testis using a less sensitive Pico system. IFT27 protein was detected only in the testis (Supplemental Fig. 1). However, when a more sensitive Femto system was used, it was found that IFT27 protein was also expressed in other somatic tissues at low levels, including the lung, kidney, liver, and spleen and brain (Fig. 1C). IFT27 protein expression level was subsequently investigated in mouse testis samples of different ages during the first wave of spermatogenesis. IFT27 protein was first visible at day 20 after birth. The expression level was dramatically increased at postnatal day 24 and remained at a high level until day 42 (Fig. 1D). Expression of IFT27 and IFT25 in epididymal sperm was examined. Even though both were expressed in the mouse testis, none of them was expressed in the sperm (Fig. 1E).

In the testis seminiferous tubules, there are germ cells and somatic cells. To investigate which cell types express IFT27, immunofluorescence staining was conducted. A strong signal was detected in the cytoplasm of spermatocytes and round spermatids, but not in the spermatogonia and Sertoli cells or interstitial cells (Fig. 2). In addition, some IFT27 signal was found to co-localize with acetylated-tubulin, a marker for cilia flagellum, near the lumen area but not in the developed sperm in the lumen, indicating that IFT27 is also present in the developing flagella (Supplemental Fig.2). Immunofluorescence staining was also conducted on the heart and muscle sections, none of these tissues expressed IFT27 (Supplemental Fig. 3).

Generation of conditional *Ift27* knockout mice

To study the role of IFT27 in mouse germ cell development, we generated male germ cell specific conditional knockout mouse models by crossing the floxed *Ift27* mice to the *Stra8-iCre* transgenic mice. All mice were genotyped by PCR using specific primer sets (Supplemental Fig. 4). Testicular IFT27 protein expression in the control and conditional *Ift27* mutant mice was examined by Western blot analysis and immunofluorescence (IF) staining using the anti-IFT27 antibody. The protein was expressed in all the control mice examined; however, no IFT27 protein was detected in all the seven conditional *Ift27* mutant mice analyzed (Fig. 3A). IF staining revealed that IFT27 protein was present in the cytoplasm of spermatocytes and round spermatids and the developing flagella of the control mice (Fig. 3B, upper panel; supplemental Fig.5); the signal was absent from the conditional *Ift27* mutant mice (Fig. 3B, lower panel).

Homozygous *Ift27* KO males were completely infertile

All of the mutant mice survived to adulthood and did not show any gross abnormalities. To examine whether disruption of *Ift27* gene in male germ cells affected fertility, 3–4 months old and 6-weeks old controls and homozygous *Ift27* mutant males were mated with 3–4 months old wild-type females for at least two months. All ten 3–4 months old and ten 6-weeks old control males showed normal fertility, and all sired normal size litters. However, all 3–4 months old and 6-weeks old mutant mice were completely infertile, and no litters were born during two months of breeding (Table 1).

Abnormally developed sperm, significantly reduced sperm count and motility in the conditional *Ift27* KO mice

To determine the factors that caused the infertility phenotype, we first examined physiological parameters of sperm collected from the cauda epididymedes. Spermatozoa from the control mice showed normal morphology, including well-shaped heads and long, smooth tails (Fig. 4Aa). However, multiple abnormalities were discovered from the sperm collected from the *Ift27* KO mice (Fig. 4Ab-h, Supplemental Fig. 6a–h), including short, bent tails and round heads. The thickness of flagella among the sperm was inconsistent, and vesicles could be observed inside the flagella for most of them. Very few sperm appeared to have a smooth tail; however, along the whole tail, different light densities were observed. Some sperm had large bulbs in the end of the tails. Sperm count from the control mice was normal, but the number was significantly reduced in the mutant mice (Fig. 4B). More than 60% sperm from the control mice were motile (Fig. 4C), and they showed progressive motility (Fig. 4D, movies A, B). However, only about 2% sperm from the *Ift27* KO mice were motile (Fig. 4C), and no sperm showed progressive motility (Fig. 4D, Supplemental movies C, D).

Abnormal sperm ultrastructure under SEM

To better illustrate the abnormal sperm morphology observed under light microscopy, SEM was conducted. Consistently, sperm from the control mice showed normally developed heads and flagella (Fig. 5-a). However, no sperm recovered from cauda epididymedes were morphologically normal (Fig. 5b–f, Supplemental Fig.7), and all displayed certain abnormalities as described above, including round and other mis-shaped heads, short tails, swollen tail tips, uneven thickness along the flagella, et al. These defects suggest an abnormal spermatogenesis process in the absence of IFT27.

Abnormal spermatogenesis in the absence of IFT27

Spermatogenesis occurs in the testis seminiferous tubule. Histology of testes of the control and *Ift27* KO mice was examined. Testis size of the mutant mice appeared to be normal, and there was no significant difference in the testis weigh and testis/body weigh between the control and the KO mice (Supplemental Fig. 8). H&E staining showed that in the control mice, step 16 spermatids line the lumen, with their long tails extending parallel into the lumen. Residual bodies (Rb) of left over cytoplasm formed between the sperm heads and step 7–8 round spermatids (Fig. 6A, Supplemental Fig. 9, left panel). However, in the *Ift27KO* mice testes, multiple signs of failure of spermatogenesis were observed in the-spermiogenesis, including abnormal tails and heads, and nuclear shape failure of the step 16 spermatids and spermiation, and little sperm in the lumen (Fig. 6B–F, Supplemental Fig. 9, right panel). The developed sperm were stored in the cauda epididymedes, histology of cauda epididymis of the control and the mutant mice was examined. The cauda epididymedes of the control mice contained well-developed spermatozoa (Supplemental Fig. 10, left panels, Supplemental Fig. 11, left panel). However, in the *Ift27* KO mice, cauda epididymis lumen was filled with abnormal sperm heads, sloughed spermatids, numerous detached sperm heads and abnormal tails (Supplemental Fig. 10, right panels, Supplemental Fig. 11, right panel).

Abnormal epididymal and testicular sperm ultrastructure under TEM

Sperm flagella are special motile cilia. Besides the core “9+2” axoneme structure, sperm also have accessary structure. To examine the core and accessary structure, TEM was conducted in both epididymal and testicular sperm. Epididymal sperm from the control mice showed normal “9+2” motile cilia axoneme structure, and accessory structures were also normally organized (Fig. 7a). However, multiple abnormalities were discovered in almost all epididymal sperm recovered from the conditional *Ift27* KO mice, including disrupted “9+2” core axoneme structure, disorganized axoneme microtubule assay, distorted membranes, misplaced and missing ODFs, fiber sheath and mitochondria sheath (Fig. 7b–h, Supplemental Fig. 12a–n).

Ultrastructure of the testicular sperm was also examined. In the control mice, similar to the epididymal sperm, TEM revealed normal core axoneme and accessory structure of testicular sperm (Fig. 8a, b). Very few axoneme structures could be seen in the seminiferous tubules from the *Ift27* KO mice (Fig. 8c). From the images of the few developed sperm, none showed normal morphology. The same defects as seen in the epididymal sperm were observed (Fig. 8c–f, and Supplemental Fig. 13a–d).

IFT27 regulates protein levels of other IFT proteins, particularly IFT25 in male germ cells. To explore the potential functional relationship between IFT27 and other IFT proteins, expression levels of selective IFT proteins in the testis were examined by Western blot analysis in the control and the *Ift27* mutant mice. Protein levels of IFT25, the IFT27 binding partner, and IFT81, a component of IFT-B complex were significantly reduced in the *Ift27* KO mice; however, protein levels of IFT20, IFT74, two additional components of the IFT-B complex, and IFT140, a component of IFT-A complex, were not changed (Fig. 9).

Sperm Lipid raft was disrupted in the conditional *Ift25* KO mice, but not *Ift27* KO mice The slightly different phenotype between conditional *Ift25* and *Ift27* KO mice prompted us to consider that the two IFT proteins may conduct slightly different functions in sperm flagella formation/function. Given that IFT25 plays a role in lipid raft status in mammalian cells (Bellyei et al, 2007), we analyzed epididymal sperm lipid rafts in the control, conditional *Ift25*, and *Ift27* KO mice. In the sperm of the control mice, lipid rafts were evenly distributed on the head surface and along the flagella, particularly the middle piece (Fig. 10A). However, in the sperm from the *Ift25* KO mice, the pattern was completely changed. In some sperm, lipid rafts were present in the heads, but the signal scattered, and almost no signal appeared in the tail (Fig. 10B). Some sperm had almost no signal in the head, but appeared to have scattered signal along the tail (Fig. 10C). In the *Ift27* KO mice, even though the sperm morphology was abnormal, lipid raft distribution appeared to be normal (Fig. 10D).

Discussion

In this study, we investigated the role of IFT27 in male germ cell development and male fertility, examined protein expression levels of selected IFT proteins in the conditional *Ift27* KO mice, and compared phenotypes between *Ift25* and *Ift27* KO mice. We discovered that similar to the *Ift25* KO mice, the *Ift27* KO mice were infertile due to severe defects in the

final phase of spermatogenesis, spermiogenesis. Some germ cells completed the spermatogenesis process and formed spermatozoa. However, like the sperm from the *Ift25* KO mice, sperm from the *Ift27* KO mice showed abnormal flagella structure, particularly the accessory structures, and most also developed abnormal heads. Unlike sperm from the *Ift25* KO mice that were completely immotile, about 2% sperm from the *Ift27* KO mice were motile with dramatically reduced motility. Sperm lipid raft, which was disrupted in the *Ift25* KO mice, appeared to be normal in the sperm from the *Ift27* KO mice.

Besides germ cells, the testis seminiferous tubules also contain somatic cells, including Leydig cells and Sertoli cells. Our IF results using the testis sections and isolated testicular cells demonstrated that IFT27 is dominantly expressed in spermatocytes/spermatids and the developing flagella other than in the somatic cells and the developed sperm, which is consistent with its predicted function IFT in cilia/flagella assembly. Given that the Cre recombinase activity is high in male germ cells of the *Stra8-iCre* mouse, we consider that the phenotype described here was largely duo to disruption of *Ift27* in the germ cells. Even though IFT27 protein was not detected in the somatic cells by IF in our study, the protein might expression at low levels in somatic cells in the testis. It is also impossible to exclude that somatic cells also express Cre recombinase activity at some level. Thus, disruption of *Ift27* in these somatic cells may also contribute to the phenotype. To study the function of IFT27 in these somatic cells, different transgenic mice should be used to specially targeting Ift27 in these cells.

Similar to the *Ift25* KO mice, the severe phenotype was unexpected. As noted, genes encoding *Ift25* and *Ift27* homologues are absent from the genomes of organisms that lack cilia and flagella and also from those of *Drosophila melanogaster* and *Caenorhabditis elegans*, indicating that IFT25 and IFT27 have a specialized role in IFT that is not required for the assembly of cilia or flagella in the worm and fly (Rual et al, 2005). This is also supported by the observations from the mouse models that *Ift25* and *Ift27* were disrupted ubiquitously. Global knockout of *Ift25* and *Ift27* resulted in multiple phenotypes related to the disruption of the Hedgehog signaling pathway localized in the primary cilia; however, ciliogenesis was not affected as demonstrated by normal cilia morphology in MEFs, tracheal epithelial cells and hair cells (Keady et al, 2012; Yang et al, 2015). Apparently, IFT25/IFT27 play different roles in the development of cilia/flagella in somatic cells and male germ cells. In the present model, *Ift27* was inactivated only in germ cells. As expected, all KO mice survived to adulthood and did not show any gross abnormalities during the whole developmental stage. However, all KO males were infertile, presumably due to both significantly reduced sperm counts and disrupted development of the sperm head/flagella structures. Only about 2% sperm from the conditional *Ift27* KO mice showed dramatically reduced motility. Under light microscopy and SEM, sperm from the *Ift27* KO and *Ift25* KO mice shared many common morphologic abnormalities, including short tails, the swollen tail tips, and flagella that had variable thicknesses along the lengths of their tails. However, the branched flagella present in the sperm from the *Ift25* KO mice were never observed in the sperm from the *Ift27* KO mice. Like the sperm from the *Ift25* KO mice, TEM also showed vesicles/vacuoles in some area along the flagella in the sperm from the *Ift27* KO mice. It is likely that the IFT mechanism is disrupted in the germ cells in the absence of IFT27, and cargo vesicles are not being transported efficiently and integrated into the developing

flagellum. A typical phenotype for ciliary retrograde transport failure is to form a bulb at the ciliary tip (Pedersen et al, 2006; Qin et al., 2004). Even though IFT25 and IFT27 are considered to be IFT-B components, and disruption of IFT-B genes usually result in short cilia/flagella (Ishikawa and Marshall, 2011; Pedersen et al, 2006; Qin et al, 2004), the swollen tail tips in the IFT27-deficient mice suggests that besides anterograde, IFT27 might also be involved in retrograde transport. This is supported by SEM studies that showed irregularities all along some of the tails, and perhaps the accumulation at the end could be failure of vesicles to attach to the appropriate destination, causing them to accumulate at the end.

It is not surprising that *Ift25* and *Ift27* KO mice shared so many common phenotypes. Recent structural analysis revealed that IFT25 and IFT27 reside in a binary complex (Bhogaraju et al, 2011). IFT25 binds to IFT27 directly in *Chlamydomonas* of humans and mice (Liu et al, 2017). In several cells/tissues of the *Ift25* KO mice, IFT27 was nearly absent (Eguether et al., 2014; Wang et al, 2009; Yang et al, 2015). On the contrary, IFT25 was still present in the *Ift27* KO mice, indicating that presence of IFT27 in these cells/tissues depends on IFT25. *Ift25* KO mice show phenotypes similar to the *Ift25/Ift27* double KOs. The *Ift25* KO mice not only showed similar phenotypes to the *Ift27* KO mice, but also displayed other phenotypes unique to the absence of IFT25, that explains why *Ift25* KO mice demonstrated more severe phenotypes than the *Ift27* KO mice in our germ cell specific disruption models. For example, sperm from the *Ift25* KO mice were completely immotile, but still about 2% sperm from the *Ift27* KO mice were motile, even though the motility was dramatically reduced. The branched sperm flagella were frequently seen in the *Ift25* KO mice, but were never seen in the *Ift27* KO mice. These slight differences between the two mutant mice suggest that IFT25 may conduct additional roles beyond IFT27, and one might be to regulate lipid raft status in sperm. Lipid rafts are specialized membrane micro-domains that function as signaling platforms across plasma membranes of many cells (George and Wu, 2012; Levental and Veatch, 2016), including sperm (Travis et al, 2001; Trevino et al., 2001). Sperm lipid rafts function in signaling upstream of cAMP synthesis, and are required for Ca(2+)-dependent pathways underlying activation in *Ciona* sperm (Zhu and Inaba, 2011). It has been shown that over-expression of IFT25 stabilizes lipid rafts in cultured mammalian cells (Bellyei et al, 2007). In the *Ift25* KO mice, sperm lipid rafts were largely disrupted; however, lipid rafts seemed to be normal in the sperm of the *Ift27* KO mice. The disrupted lipid rafts may contribute partially to more sever phenotype discovered in the *Ift25* KO mice. In addition, IFT25 might carry additional cargos that are not transported by the IFT25/IFT27 complex.

Even though IFT25 and IFT27 form a complex, it is highly possible that IFT25 forms another IFT complex without IFT27. We previously analyzed protein levels of selected IFT proteins in the *Ift25* KO mice, and discovered that IFT20 and IFT81 levels were reduced. Protein levels of the same IFT proteins were examined in the conditional *Ift27* KO mice. Similar to the *Ift25* KO mice, testicular IFT81 level was also reduced in the *Ift27* KO mice. Surprisingly, IFT20 level, which was also reduced in the *Ift25* KO mice, was not changed in the *Ift27* KO mice, indicating that IFT25 and IFT27 have a different role in determining testicular IFT20 protein level. IFT25 might form a complex containing IFT20 but not IFT27. Like IFT25 and IFT27, IFT20 is also a component of IFT-B complex (Follit et al, 2009). Our

earlier studies demonstrated that IFT20 is also a key factor to control mouse spermiogenesis (Zhang et al, 2016). Thus, down-regulation of IFT20 in the conditional *Ift25* knockout mice may contribute partially to the slight different phenotype between *Ift25* and *Ift27* knockout mice.

Given that both IFT25 and IFT27 are not required in ciliogenesis in somatic cells (Eguether et al, 2014; Yang et al, 2015), but little is known about their roles in the spermatogenesis in mice. As we discussed previously in our conditional *Ift25* knockout studies that IFT25 may be responsible to transport protein components unique for sperm flagella (Liu et al, 2017). This is probably also true for IFT27, which is supported by the common phenotypes in general and almost identical ultra-structural changes in sperm of *Ift25* and *Ift27* KO mice.

Like the conditional *Ift25* KO mice, besides disruption of sperm accessory structures, TEM studies also demonstrated defects of core axonemal structures in the sperm of the *Ift27* KO mice. One possibility is that IFT25/IFT27 does play a role in assembling the core axoneme structure of sperm, which is different from their roles the somatic cells where they do not modulate ciliogenesis. Another possibility is that the defects of the core axoneme structure are secondary to the defects of the accessory structures, which was reported in the CABYR mutant mice (Young et al., 2016), in which the axoneme defect was caused by defects of fibrous sheath.

Even though our antibody successfully detected IFT27 protein in the round spermatids, the antibody failed to detect the protein in germ cells at a later stage. We assume it should be present in the locations related to sperm flagella formation, such as the manchette, a structure proposed to transporting cargo proteins for flagella formation (Kierszenbaum and Tres, 2004; Lehti and Sironen, 2016); the basal bodies, the template for flagella formation (Marshall, 2008); and the developing flagella in the elongating spermatids. Thus, other specific antibodies should be generated to target IFT27 in male germ cells.

Conclusions

Overall, we studied the role of IFT27 in male germ cells, and compared its role with IFT25, its binding partner, and discovered that like IFT25, even though IFT27 is not required for cilia formation in somatic cells, it is indispensable for sperm flagella formation, sperm motility and male fertility. By working together with IFT25, IFT27 might conduct multiple functions in germ cells' development and flagella formation through assembling accessory structures, sperm unique ion channels, and ATPases for normal sperm function.

Supplementary Material

Refer to Web version on PubMed Central for supplementary material.

Acknowledgments

We thank Dr. Scott C. Henderson, and Judy C. Williamson for their assistance with using the electronic microscopy in Microscopy Core Facility of Virginia Commonwealth University.

References

Aldahmesh MA, Li Y, Alhashem A, Anazi S, Alkuraya H, Hashem M, Awaji AA, Sogaty S, Alkharashi A, Alzahrani S, Al Hazzaa SA, Xiong Y, Kong S, Sun Z, Alkuraya FS. IFT27, encoding a small GTPase component of IFT particles, is mutated in a consanguineous family with Bardet-Biedl syndrome. Hum Mol Genet. 2014; 23:3307–3315. [PubMed: 24488770]

Barker AR, Thomas R, Dawe HR. Meckel-Gruber syndrome and the role of primary cilia in kidney, skeleton, and central nervous system development. Organogenesis. 2014; 10:96–107. [PubMed: 24322779]

Bellyei S, Szigeti A, Boronkai A, Pozsgai E, Gomori E, Melegh B, Janaky T, Bognar Z, Hocsak E, Sumegi B, Gallyas F Jr. Inhibition of cell death by a novel 16.2 kD heat shock protein predominantly via Hsp90 mediated lipid rafts stabilization and Akt activation pathway. Apoptosis. 2007; 12:97–112. [PubMed: 17136496]

Bhogaraju S, Taschner M, Morawetz M, Basquin C, Lorentzen E. Crystal structure of the intraflagellar transport complex 25/27. EMBO J. 2011; 30:1907–1918. [PubMed: 21505417]

Eguether T, San Agustin JT, Keady BT, Jonassen JA, Liang Y, Francis R, Tobita K, Johnson CA, Abdelhamed ZA, Lo CW, Pazour GJ. IFT27 links the BBSome to IFT for maintenance of the ciliary signaling compartment. Dev Cell. 2014; 31:279–290. [PubMed: 25446516]

Follit JA, Xu F, Keady BT, Pazour GJ. Characterization of mouse IFT complex B. Cell Motil Cytoskeleton. 2009; 66:457–468. [PubMed: 19253336]

Forsythe, E., Beales, PL. Bardet-Biedl Syndrome. Pagon, RA.Adam, MP.Ardinger, HH.Wallace, SE.Amemiya, A.Bean, LJH.Bird, TD.Ledbetter, N.Mefford, HC.Smith, RJH., Stephens, K., editors. GeneReviews(R); Seattle (WA): 1993.

George KS, Wu S. Lipid raft: A floating island of death or survival. Toxicol Appl Pharmacol. 2012; 259:311–319. [PubMed: 22289360]

Hou Y, Witman GB. Dynein and intraflagellar transport. Exp Cell Res. 2015; 334:26–34. [PubMed: 25725253]

Huet D, Blisnick T, Perrot S, Bastin P. The GTPase IFT27 is involved in both anterograde and retrograde intraflagellar transport. Elife. 2014; 3:e02419. [PubMed: 24843028]

Ishikawa H, Marshall WF. Ciliogenesis: building the cell's antenna. Nat Rev Mol Cell Biol. 2011; 12:222–234. [PubMed: 21427764]

Ishikawa H, Marshall WF. Intraflagellar Transport and Ciliary Dynamics. Cold Spring Harb Perspect Biol. 2017; 9

Jonassen JA, SanAgustin J, Baker SP, Pazour GJ. Disruption of IFT complex A causes cystic kidneys without mitotic spindle misorientation. J Am Soc Nephrol. 2012; 23:641–651. [PubMed: 22282595]

Keady BT, Samtani R, Tobita K, Tsuchya M, San Agustin JT, Follit JA, Jonassen JA, Subramanian R, Lo CW, Pazour GJ. IFT25 links the signal-dependent movement of Hedgehog components to intraflagellar transport. Dev Cell. 2012; 22:940–951. [PubMed: 22595669]

Kierszenbaum AL, Tres LL. The acrosome-acroplaxome-manchette complex and the shaping of the spermatid head. Arch Histol Cytol. 2004; 67:271–284. [PubMed: 15700535]

Lechtreck KF, Luro S, Awata J, Witman GB. HA-tagging of putative flagellar proteins in Chlamydomonas reinhardtii identifies a novel protein of intraflagellar transport complex B. Cell Motil Cytoskeleton. 2009; 66:469–482. [PubMed: 19382199]

Lehman JM, Laag E, Michaud EJ, Yoder BK. An essential role for dermal primary cilia in hair follicle morphogenesis. J Invest Dermatol. 2009; 129:438–448. [PubMed: 18987668]

Lehti MS, Sironen A. Formation and function of the manchette and flagellum during spermatogenesis. Reproduction. 2016; 151:R43–54. [PubMed: 26792866]

Levental I, Veatch SL. The Continuing Mystery of Lipid Rafts. J Mol Biol. 2016; 428:4749–4764. [PubMed: 27575334]

Liew GM, Ye F, Nager AR, Murphy JP, Lee JS, Aguiar M, Breslow DK, Gygi SP, Nachury MV. The intraflagellar transport protein IFT27 promotes BBSome exit from cilia through the GTPase ARL6/BBS3. Dev Cell. 2014; 31:265–278. [PubMed: 25443296]

Liu H, Li W, Zhang Y, Zhang Z, Shang X, Zhang L, Zhang S, Li Y, Somoza AV, Delpi B, Gerton GL, Foster JA, Hess RA, Pazour GJ, Zhang Z. IFT25, an intraflagellar transporter protein dispensable for ciliogenesis in somatic cells, is essential for sperm flagella formation. uBiol Reprod. 2017

Lucker BF, Behal RH, Qin H, Siron LC, Taggart WD, Rosenbaum JL, Cole DG. Characterization of the intraflagellar transport complex B core: direct interaction of the IFT81 and IFT74/72 subunits. J Biol Chem. 2005; 280:27688–27696. [PubMed: 15955805]

Marshall WF. Basal bodies platforms for building cilia. Curr Top Dev Biol. 2008; 85:1–22. [PubMed: 19147000]

Marszalek JR, Ruiz-Lozano P, Roberts E, Chien KR, Goldstein LS. Situs inversus and embryonic ciliary morphogenesis defects in mouse mutants lacking the KIF3A subunit of kinesin-II. Proc Natl Acad Sci U S A. 1999; 96:5043–5048. [PubMed: 10220415]

McDonald K. Osmium ferricyanide fixation improves microfilament preservation and membrane visualization in a variety of animal cell types. J Ultrastruct Res. 1984; 86:107–118. [PubMed: 6539826]

Mourao A, Christensen ST, Lorentzen E. The intraflagellar transport machinery in ciliary signaling. Curr Opin Struct Biol. 2016; 41:98–108. [PubMed: 27393972]

Nissen S, Liang S, Shehktman T, Kelsoe JR, Bipolar Genome S, Greenwood TA, Nievergelt CM, McKinney R, Shilling PD, Smith EN, Schork NJ, Bloss CS, Nurnberger JI Jr, Edenberg HJ, Foroud T, Koller DL, Gershon ES, Liu C, Badner JA, Scheftner WA, Lawson WB, Nwulia EA, Hipolito M, Coryell W, Rice J, Byerley W, McMahon FJ, Berrettini WH, Potash JB, Zandi PP, Mahon PB, McInnis MG, Zollner S, Zhang P, Craig DW, Szelinger S, Barrett TB, Schulze TG. Evidence for association of bipolar disorder to haplotypes in the 22q12.3 region near the genes stargazin, IFT27 and parvalbumin. Am J Med Genet B Neuropsychiatr Genet. 2012; 159B:941–950. [PubMed: 23038240]

Nonaka S, Tanaka Y, Okada Y, Takeda S, Harada A, Kanai Y, Kido M, Hirokawa N. Randomization of left-right asymmetry due to loss of nodal cilia generating leftward flow of extraembryonic fluid in mice lacking KIF3B motor protein. Cell. 1998; 95:829–837. [PubMed: 9865700]

Nozaki S, Katoh Y, Terada M, Michisaka S, Funabashi T, Takahashi S, Kontani K, Nakayama K. Regulation of ciliary retrograde protein trafficking by the Joubert syndrome proteins ARL13B and INPP5E. J Cell Sci. 2017; 130:563–576. [PubMed: 27927754]

Pazour GJ, Baker SA, Deane JA, Cole DG, Dickert BL, Rosenbaum JL, Witman GB, Besharse JC. The intraflagellar transport protein, IFT88, is essential for vertebrate photoreceptor assembly and maintenance. J Cell Biol. 2002; 157:103–113. [PubMed: 11916979]

Pedersen LB, Geimer S, Rosenbaum JL. Dissecting the molecular mechanisms of intraflagellar transport in chlamydomonas. Curr Biol. 2006; 16:450–459. [PubMed: 16527740]

Prevo B, Scholey JM, Peterman EJG. Intraflagellar transport: mechanisms of motor action, cooperation, and cargo delivery. FEBS J. 2017

Qin H, Diener DR, Geimer S, Cole DG, Rosenbaum JL. Intraflagellar transport (IFT) cargo: IFT transports flagellar precursors to the tip and turnover products to the cell body. J Cell Biol. 2004; 164:255–266. [PubMed: 14718520]

Qin H, Wang Z, Diener D, Rosenbaum J. Intraflagellar transport protein 27 is a small G protein involved in cell-cycle control. Curr Biol. 2007; 17:193–202. [PubMed: 17276912]

Rual JF, Venkatesan K, Hao T, Hirozane-Kishikawa T, Dricot A, Li N, Berriz GF, Gibbons FD, Dreze M, Ayivi-Guedehoussou N, Klitgord N, Simon C, Boxem M, Milstein S, Rosenberg J, Goldberg DS, Zhang LV, Wong SL, Franklin G, Li S, Albala JS, Lim J, Fraughton C, Llamosas E, Cevik S, Bex C, Lamesch P, Sikorski RS, Vandenhaute J, Zoghbi HY, Smolyar A, Bosak S, Sequerra R, Doucette-Stamm L, Cusick ME, Hill DE, Roth FP, Vidal M. Towards a proteome-scale map of the human protein-protein interaction network. Nature. 2005; 437:1173–1178. [PubMed: 16189514]

Sadate-Ngatchou PI, Payne CJ, Dearth AT, Braun RE. Cre recombinase activity specific to postnatal, premeiotic male germ cells in transgenic mice. Genesis. 2008; 46:738–742. [PubMed: 18850594]

San Agustin JT, Pazour GJ, Witman GB. Intraflagellar transport is essential for mammalian spermiogenesis but is absent in mature sperm. Mol Biol Cell. 2015; 26:4358–4372. [PubMed: 26424803]

Scholey JM. Kinesin-2: a family of heterotrimeric and homodimeric motors with diverse intracellular transport functions. Annu Rev Cell Dev Biol. 2013; 29:443–469. [PubMed: 23750925]

Srivastava S, Sayer JA. Nephronophthisis. J Pediatr Genet. 2014; 3:103–114. [PubMed: 27625867]

Su X, Driscoll K, Yao G, Raed A, Wu M, Beales PL, Zhou J. Bardet-Biedl syndrome proteins 1 and 3 regulate the ciliary trafficking of polycystic kidney disease 1 protein. Hum Mol Genet. 2014; 23:5441–5451. [PubMed: 24939912]

Suspitsin EN, Imyanitov EN. Bardet-Biedl Syndrome. Mol Syndromol. 2016; 7:62–71. [PubMed: 27385962]

Travis AJ, Merdiushev T, Vargas LA, Jones BH, Purdon MA, Nipper RW, Galatioto J, Moss SB, Hunnicutt GR, Kopf GS. Expression and localization of caveolin-1, and the presence of membrane rafts, in mouse and Guinea pig spermatozoa. Dev Biol. 2001; 240:599–610. [PubMed: 11784086]

Trevino CL, Serrano CJ, Beltran C, Felix R, Darszon A. Identification of mouse trp homologs and lipid rafts from spermatogenic cells and sperm. FEBS Lett. 2001; 509:119–125. [PubMed: 11734218]

Wang Z, Fan ZC, Williamson SM, Qin H. Intraflagellar transport (IFT) protein IFT25 is a phosphoprotein component of IFT complex B and physically interacts with IFT27 in Chlamydomonas. PLoS One. 2009; 4:e5384. [PubMed: 19412537]

Watanabe H, Kondoh G. Mouse sperm undergo GPI-anchored protein release associated with lipid raft reorganization and acrosome reaction to acquire fertility. J Cell Sci. 2011; 124:2573–2581. [PubMed: 21750187]

Wood CR, Wang Z, Diener D, Zones JM, Rosenbaum J, Umen JG. IFT proteins accumulate during cell division and localize to the cleavage furrow in Chlamydomonas. PLoS One. 2012; 7:e30729. [PubMed: 22328921]

Yang N, Li L, Eguether T, Sundberg JP, Pazour GJ, Chen J. Intraflagellar transport 27 is essential for hedgehog signaling but dispensable for ciliogenesis during hair follicle morphogenesis. Development. 2015; 142:2194–2202. [PubMed: 26023097]

Young SA, Miyata H, Satouh Y, Aitken RJ, Baker MA, Ikawa M. CABYR is essential for fibrous sheath integrity and progressive motility in mouse spermatozoa. J Cell Sci. 2016; 129:4379–4387. [PubMed: 27802166]

Zhang Z, Li W, Zhang Y, Zhang L, Teves ME, Liu H, Strauss JF 3rd, Pazour GJ, Foster JA, Hess RA, Zhang Z. Intraflagellar transport protein IFT20 is essential for male fertility and spermiogenesis in mice. Mol Biol Cell. 2016

Zhang Z, Shen X, Gude DR, Wilkinson BM, Justice MJ, Flickinger CJ, Herr JC, Eddy EM, Strauss JF 3rd. MEIG1 isfessential for spermiogenesis in mice. Proc Natl Acad Sci U S A. 2009; 106:17055–17060. [PubMed: 19805151]

Zhu L, Inaba K. Lipid rafts function in Ca2+ signaling responsible for activation of sperm motility and chemotaxis in the ascidian Ciona intestinalis. Mol Reprod Dev. 2011; 78:920–929. [PubMed: 21887722]

Highlight

We studied the role of IFT27 in male germ cells, and compared its role with IFT25, its binding partner, and discovered that like IFT25, even though IFT27 is not required for cilia formation in somatic cells, it is indispensable for sperm flagella formation, sperm motility and male fertility. By working together with IFT25, IFT27 might conduct multiple functions in germ cells' development and flagella formation through assembling accessory structures, sperm unique ion channels, and ATPases for normal sperm function.

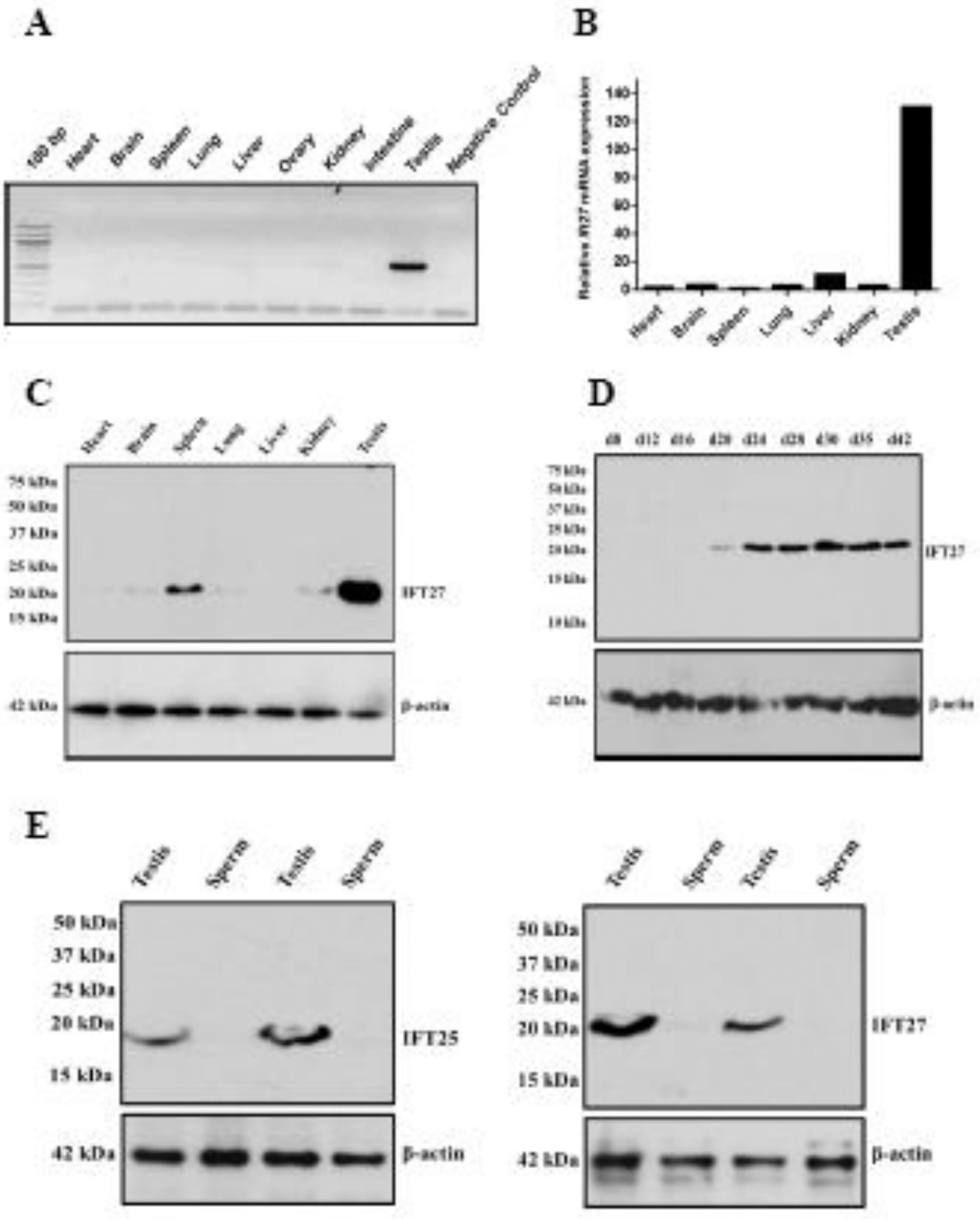

Figure 1. *Ift27* mRNA and protein are abundant in the mouse testis

A. Analysis of *Ift27* mRNA expression in multiple mouse tissues by RT-PCR. Notice that *Ift27* mRNA is highly expressed only in the testis. B. Comparison of *Ift27* mRNA expression levels in mouse tissues by qPCR. Testis has the highest expression level among the tissues examined. C. IFT27 protein expression in the indicated mouse tissues examined by Western blot analysis using the high sensitive Femto system. 10 μg of testis extract was loaded instead of 50 μg in other tissues. IFT27 is only highly abundant in the testis, it is also expressed at low level in other somatic tissues. D. IFT27 protein expression during the first wave of spermatogenesis. Notice that the protein is up-regulated from day 24 after birth,

when spermatogenesis enters the final phase, spermiogenesis. E. IFT25 and IFt27 are not expressed in the epididymal sperm. Notice that both IFT25 and IFT27 are expressed in the mouse testis, but not in the epididymal sperm.

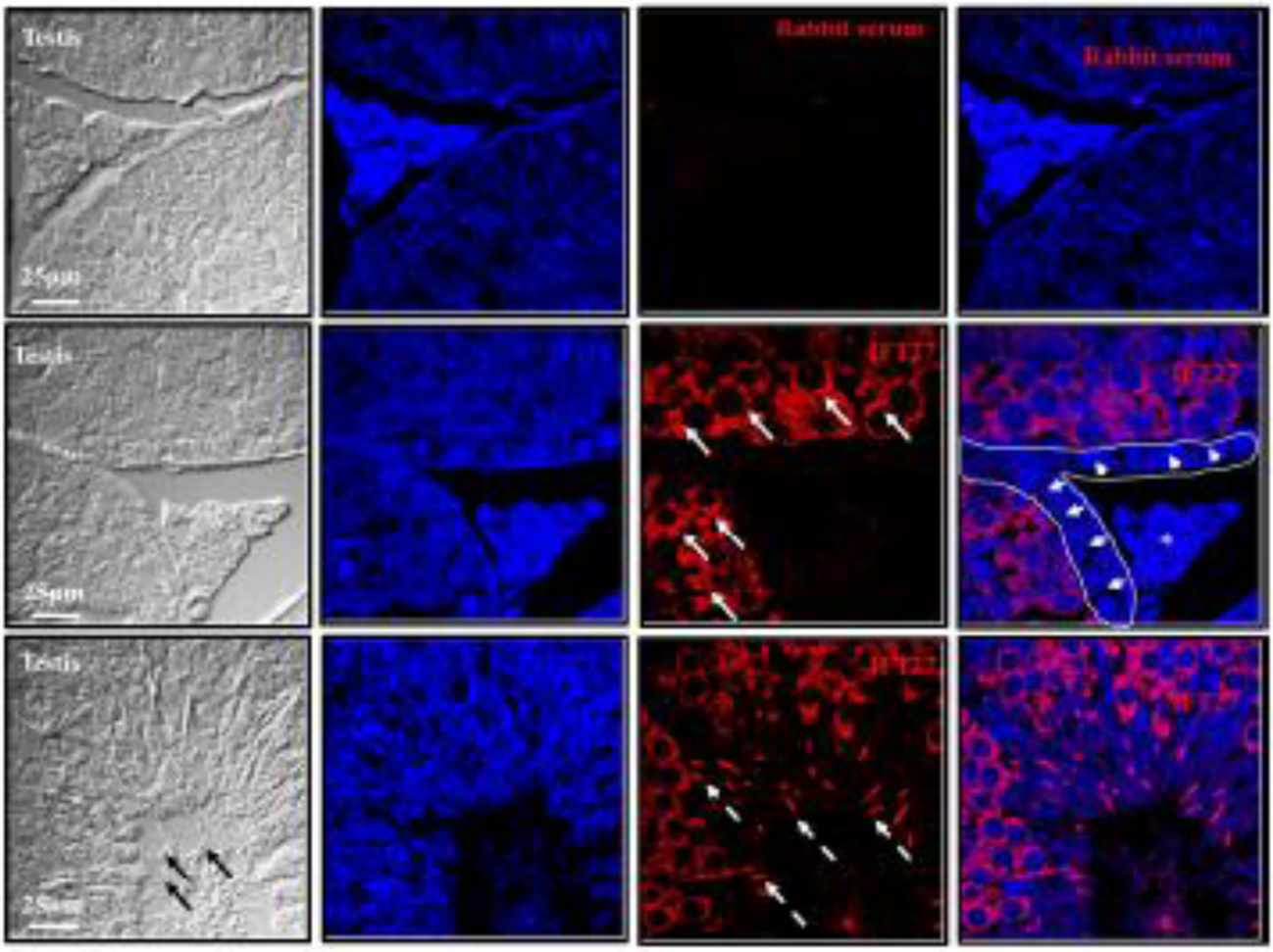

Figure 2. Localization of IFT27 in the testicular seminiferous tubules

Upper panel: The section was stained with a serum from a pre-immune rabbit; the middle and lower panels: the sections were stained with an anti-IFT27 rabbit serum. Notice that no specific signal was detected when the pre-immune rabbit serum was used. However, specific signal was visualized only in germ cells when the anti-IFT27 rabbit serum was used. The white arrows in the middle panel point to the spermatocytes/round spermatids; the dashed white arrows point to the developing flagella of the elongating spermatids. IFT27 signal was not detected in spermatogonia/Sertoli cells (white arrow heads in the circled area in the middle panel), and developed sperm in the lumen (black arrows in the lower panel). The interstitial cells that contain Leydig cells were also negative for IFT27 (white star in the middle panel).

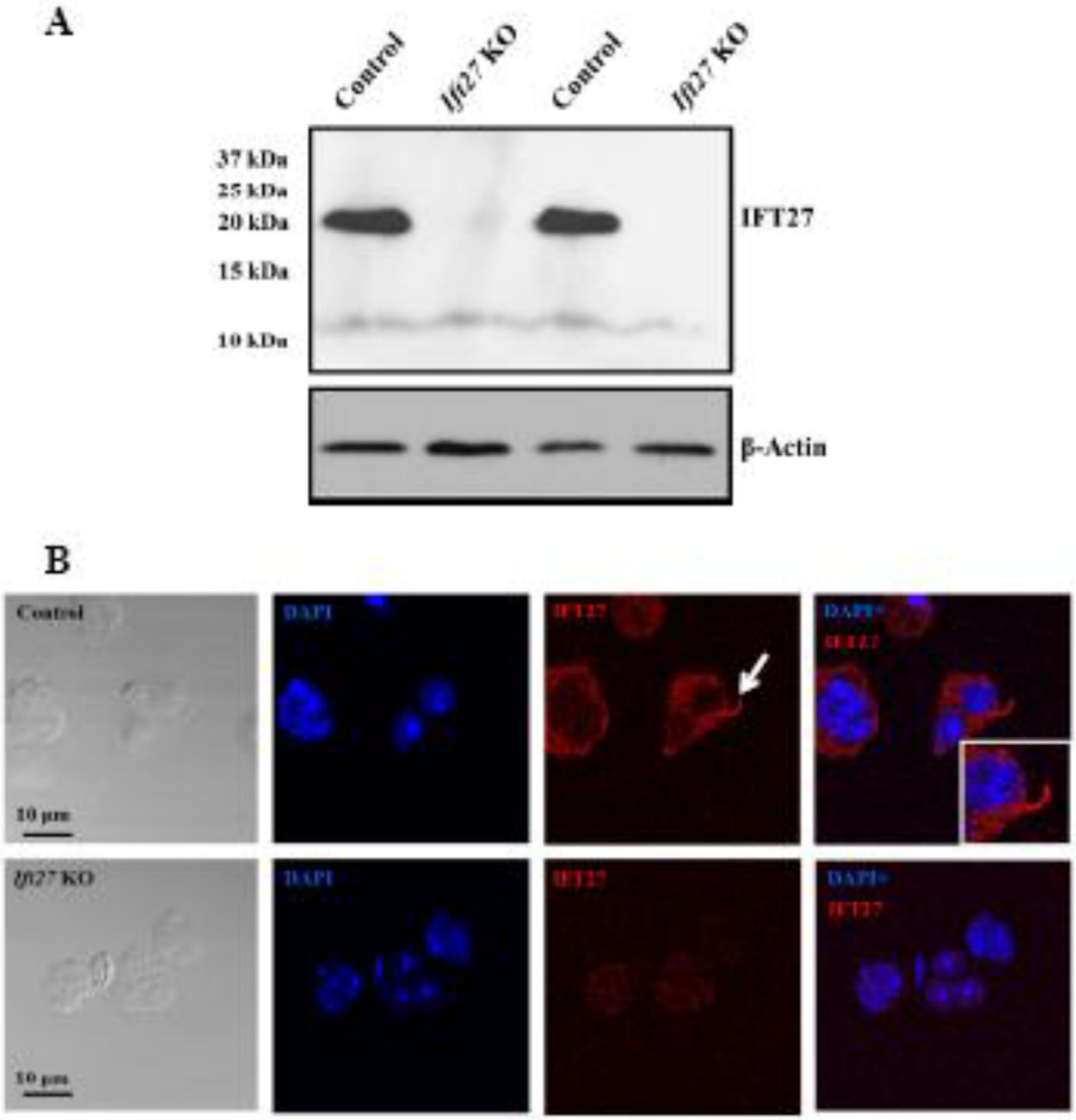

Figure 3. Generation of the conditional *Ift27* mutant mice

A. Representative Western blot result showing IFT27 protein expression in the testes of the control and the conditional mutant mice. Notice that the protein is completely missing in the mutant mice. B. Immunofluorescence result showing that IFT27 protein in present in the cytoplasm of spermatocytes and round spermatids and the developing flagella (white arrow) of the control mice; however, the specific signal is missing from the mutant mice.

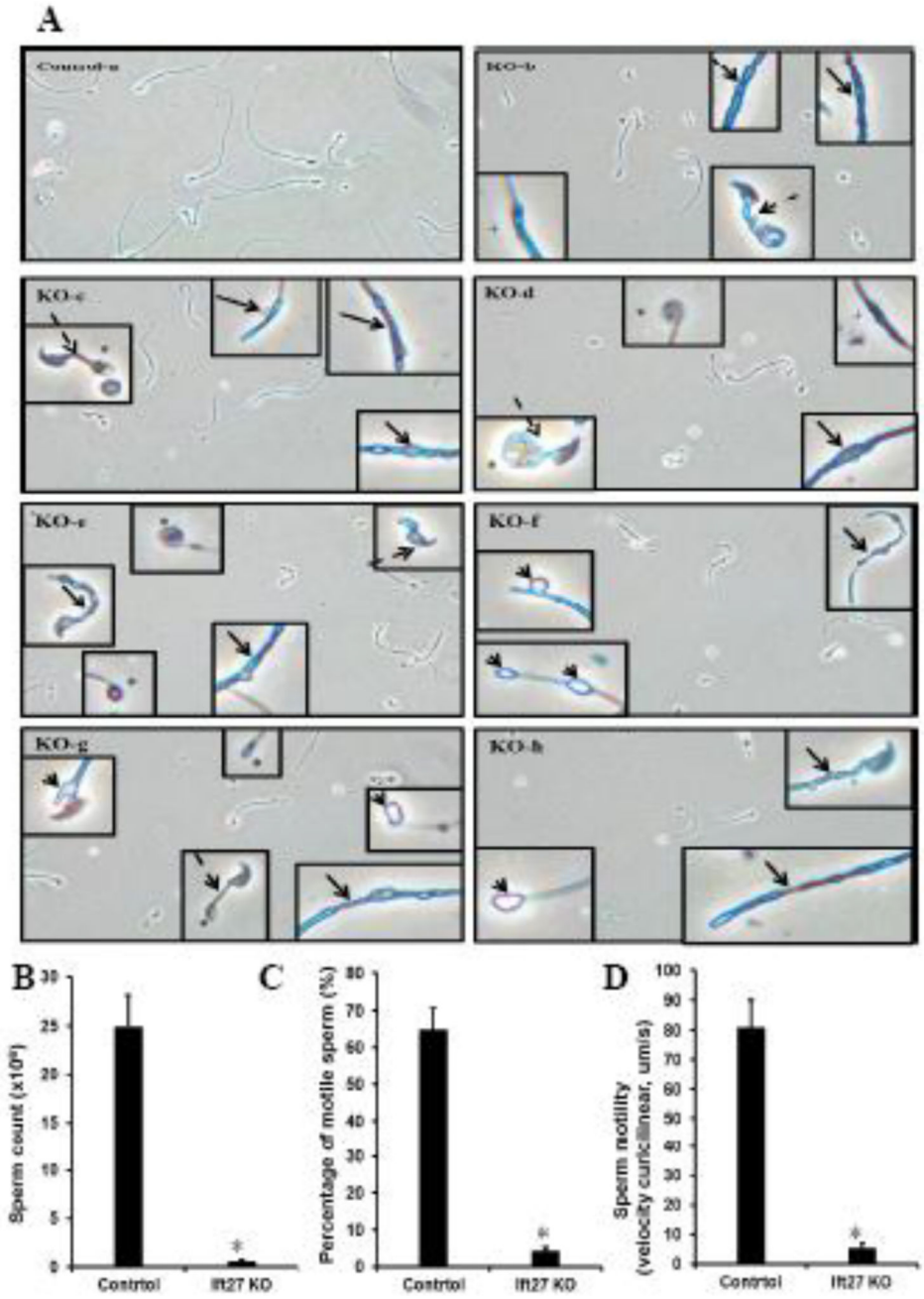

Figure 4. Abnormal sperm morphology, significantly reduced sperm count and sperm mobility in the conditional *Ift27* mutant mice

A. Representative images of epididymal sperm under a light microscopy from the control (a) and conditional *Ift27* mutant mice (b–h). Notice that very few sperm were seen in the conditional *Ift25* mutant mice under the same dilution, Sperm from the mutant mice usually had shorter tails (dashed arrows), tails with uneven thickness (arrows), vesicles (arrowheads); swollen tail tips (*), and tails with different light density (+). B. Significantly reduced sperm count in the conditional *Ift27* mutant mice; C. Significantly reduced percentage of motile sperm in the mutant mice. D. Sperm motility was significantly reduced in the sperm with motility from the *Ift27* mutant mice.

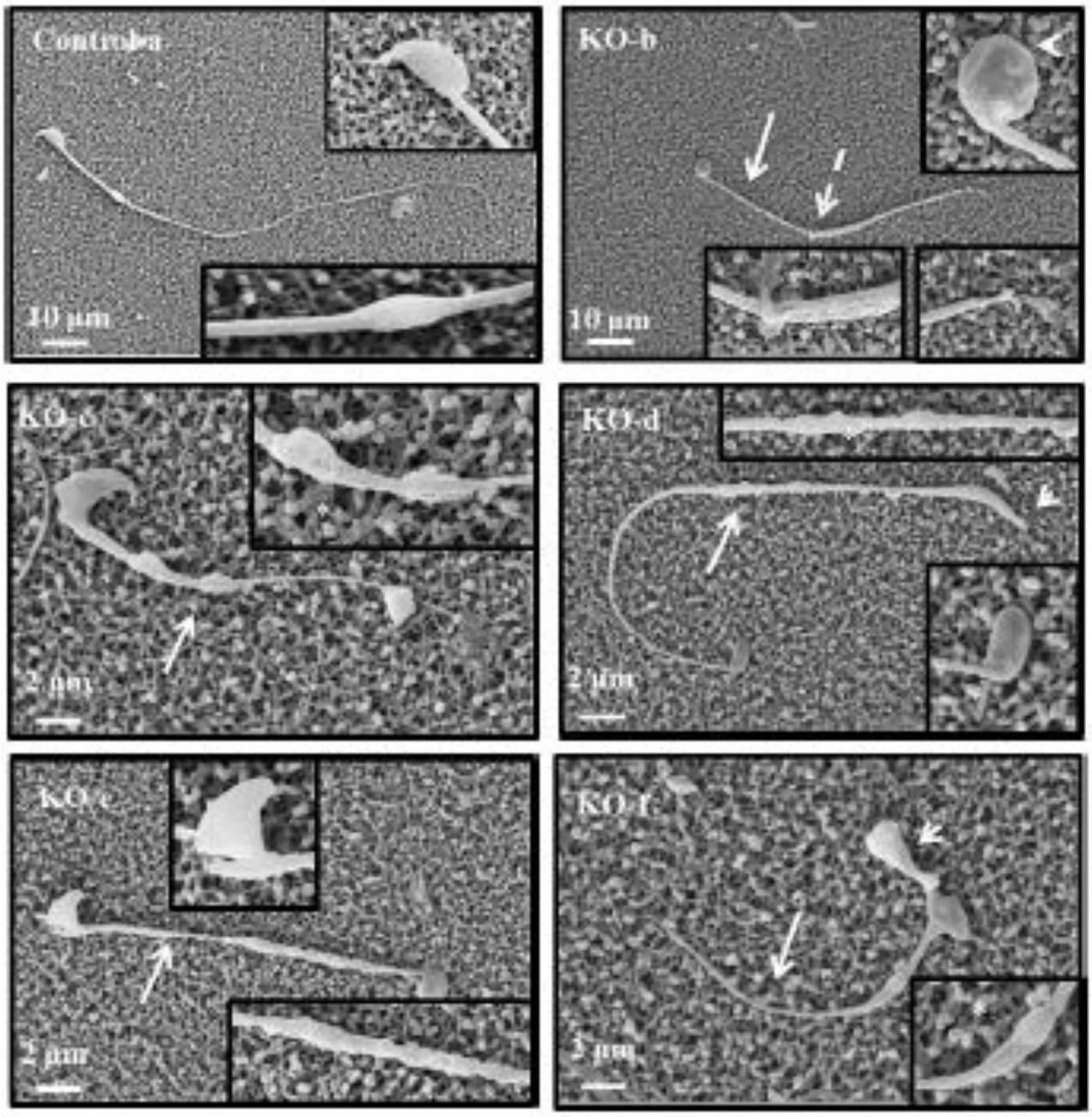

Figure 5. Analysis of epididymal sperm morphology by SEM

a: Representative image of epididymis sperm from a control mouse. The sperm has a long and smooth tail and normally shaped head. b to f: Representative images of epididymis sperm from a mutant mouse. Variety of abnormal morphology of sperm from the mutant mice. Some have short (arrows) and kinked (dashed arrow) tails, some have round and other misshaped heads (arrowheads), some have relatively longer but uneven tails (*); some have abnormal tail tips (+).

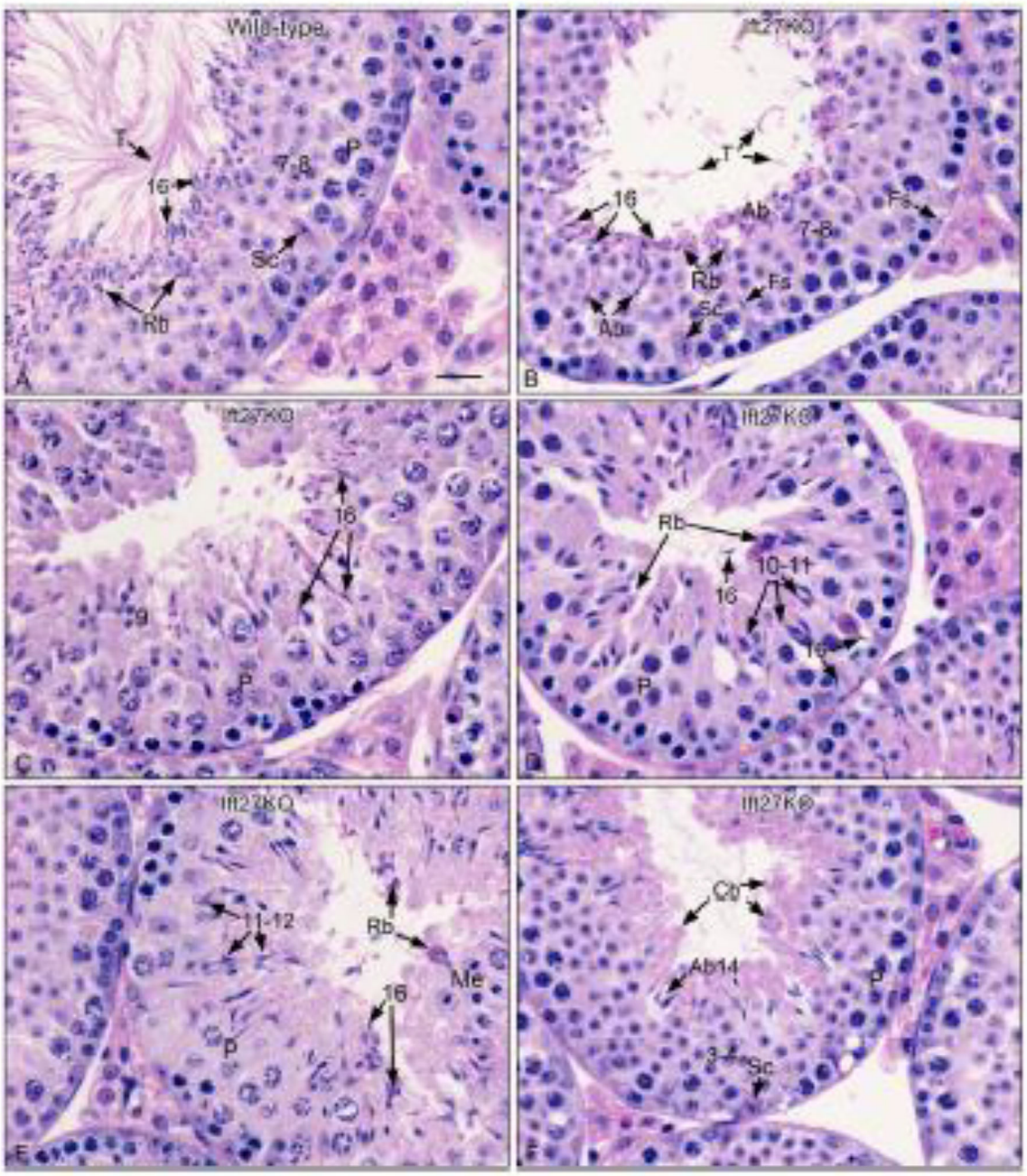

Figure 6. Histology of testes from the control and the conditional *Ift27* mutant mice

A. Wild-type testis showing stage VII-VIII. Step 16 spermatids line the lumen, with their long tails (T) extending parallel into the lumen. Residual bodies (Rb) of left over cytoplasm are forming between the sperm heads and step 7–8 round spermatids. Sc, Sertoli cell; P, pachytene spermatocytes. Bar=20μm. B–F. *Ift27KO* mice testes. B. Stage VII-VIII, showing abnormal tail (T) formation from the step 16 spermatids. Abnormal step 16 spermatid heads (Ab) are present above the nuclei of step 7–8 round spermatids. Residual bodies (Rb) are forming between the sperm heads and step 7–8 round spermatids. Sc, Sertoli cell; Fs, failed spermiation of mature sperm. C. Stage IX, showing failure of spermiation with step 16

spermatid head being retained within the seminiferous epithelium and among the step 9–10 spermatids that are just beginning to change shape. P, pachytene spermatocytes. D. Stage X-XI, showing step 16 spermatid head being retained in the epithelium along with step 10–11 spermatids having large variation in shape, with the beginning of abnormal formations. P, pachytene spermatocytes. Residual bodies of cytoplasm (Rb) are found within the epithelium. E. Stage XII, showing Step 16 spermatid head being retained in the epithelium and abnormal step 11–12 spermatids with alterations in nuclear shape. Me, spermatocytes in meiotic division. P, pachytene spermatocytes. F. Stage III-IV, showing numerous step 14 elongating spermatid heads, with some having abnormal head shapes (Ab14). Step 3–4 round spermatid nuclei are normal in appearance. Sc, Sertoli cell; P, pachytene spermatocyte.

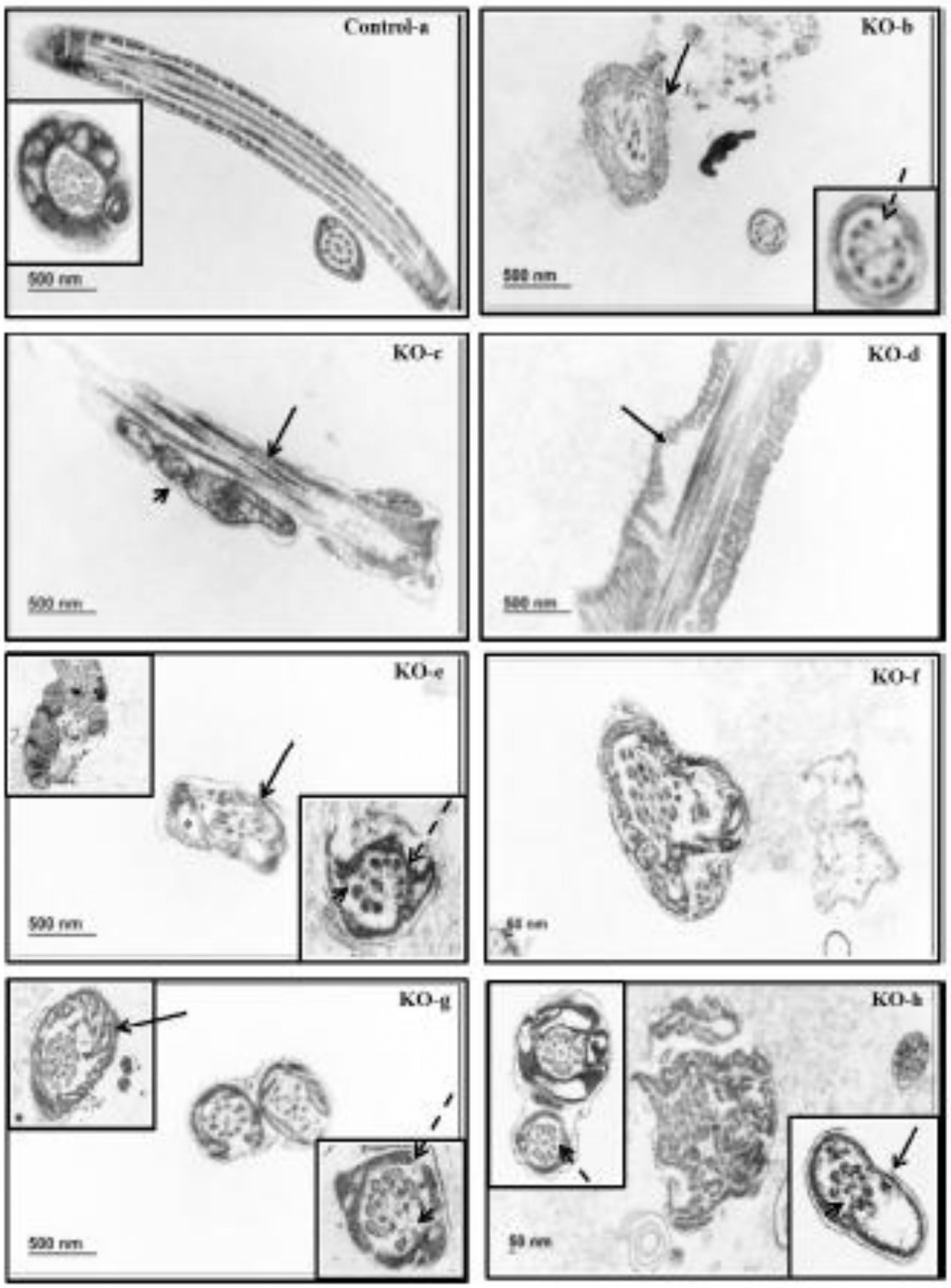

Figure 7. Analysis of epididymal sperm of the control and *Ift27* mutant mice by TEM

Sperm from the control mice show normal core "9+2" axoneme and accessary structure (a). However, sperm from the *Ift27* KO (b to h) demonstrate multiple abnormalities in both core axoneme and accessory structures. The arrow in "b" points to a very messed-up axoneme, and the arrowhead points to an axoneme missing an outer microtubule doublet; the arrow in "c" points to a flagellum with disorganized microtubule array, and the arrowhead points to several vesicles under cell membrane; the arrow in "d" points to a flagellum with distorted fibrous sheath; the arrow in "e" points to a flagellum with multiple abnormalities, including disrupted "9+2' core axoneme structure, damaged cell membrane, and a large vesicle inside

the flagellum (with a *); the left, upper insert indicates a flagellum with mis-organized mitochondria sheath, the dashed arrow point to an axoneme with broken fibrous sheath, and the arrowhead points to the axoneme missing several outer microtubules and outer dense fibers; the “*” in “f” indicates a flagellum with distorted accessory structure; the arrow in “g” points to a flagellum with disrupted fibrous sheath, the dashed arrow points to broken fibrous sheath, and the arrowhead points to the axoneme without the central microtubule and mis-organized outer dense fibers; “h” shows a flagellum with mis-organized fibrous sheath, and the dashed arrow points to an axoneme with normal looking fibrous sheath, but reduced outer dense fibers; the arrow points to broken cell membrane, and the arrowhead points to an axoneme missing several outer microtubule doublets.

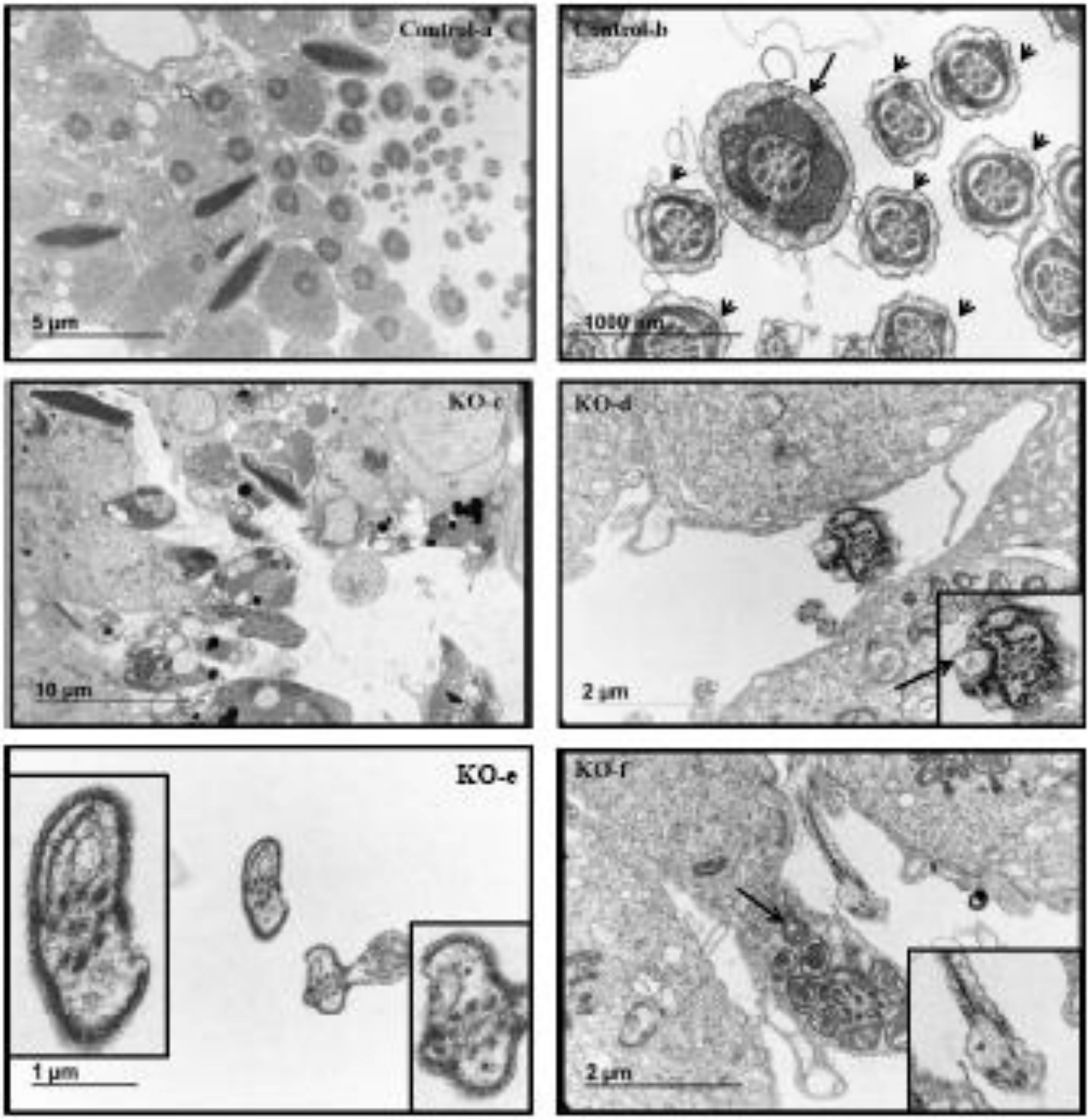

Figure 8. Analysis of testicular sperm of the control and *Ift27* mutant mice by TEM

TEM images of testicular sperm from the control (a, b) and KO (c–f) mice. In the control mice, sperm axoneme structure was easily discovered in the lumen of seminiferous tubules (a), and the ultrastructure was normal (b). The arrow pointed to an axoneme at middle piece showing normal core axoneme structure, ODF and mitochondria, and the arrow heads pointed to the axoneme at principle piece showing normal axoneme core structure, ODF and fibrous sheath. However, few sperm were discovered in the KO (c), and the sperm usually had disorganized core axoneme and accessary structures (d–f). The black arrow in “d” pointed to an axoneme with a large vacuole in the flagellum and distorted cell membrane

and fibrous sheath; the left inset in “e” showed an axoneme with disrupted core axoneme structure and disorganized fibrous sheath; the right insert indicated an axoneme with distorted cell membrane with significantly increased distance between the core axoneme and cell membrane (labeled with two stars); the black arrow in “f” pointed to an axoneme with mis-organized mitochondria sheath; and the insert showed an axoneme with a large vacuole (labeled with a *) in the flagellum.

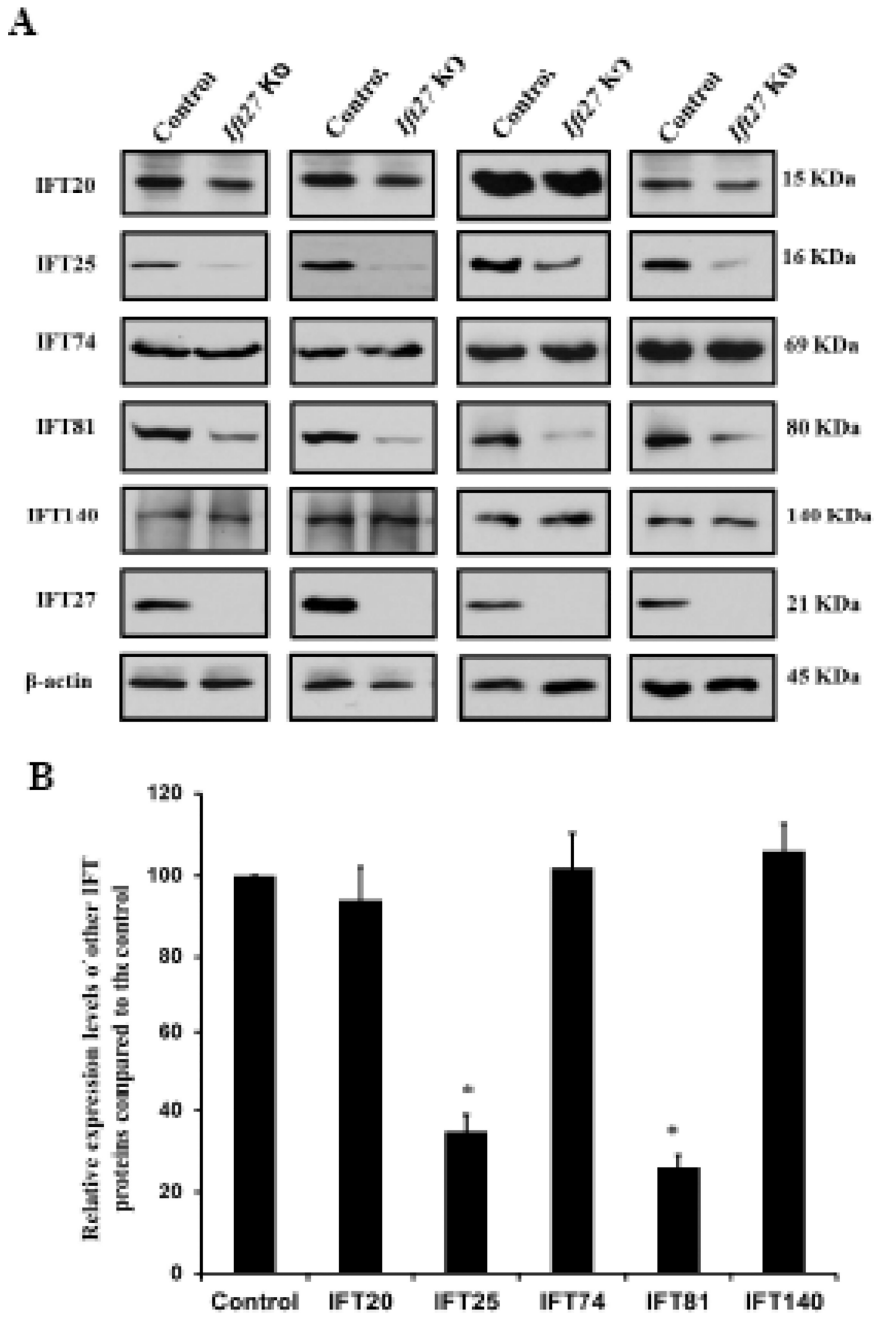

Figure 9. Protein levels of selective IFT components in the testis of control and conditional *Ift27* KO mice

A. Representative western blotting results using the indicated IFT antibodies. Notice that testicular expression of IFT25 and IFT81 reduced in the KO. B. Statistical analysis of relative expression of the IFT proteins normalized by β-actin. There is no difference in expression levels of IFT20, IFT74 and IFT140 between the controls and the *Ift25* KO mice. IFT25 and IFT81 expression levels are significantly reduced in the KO.

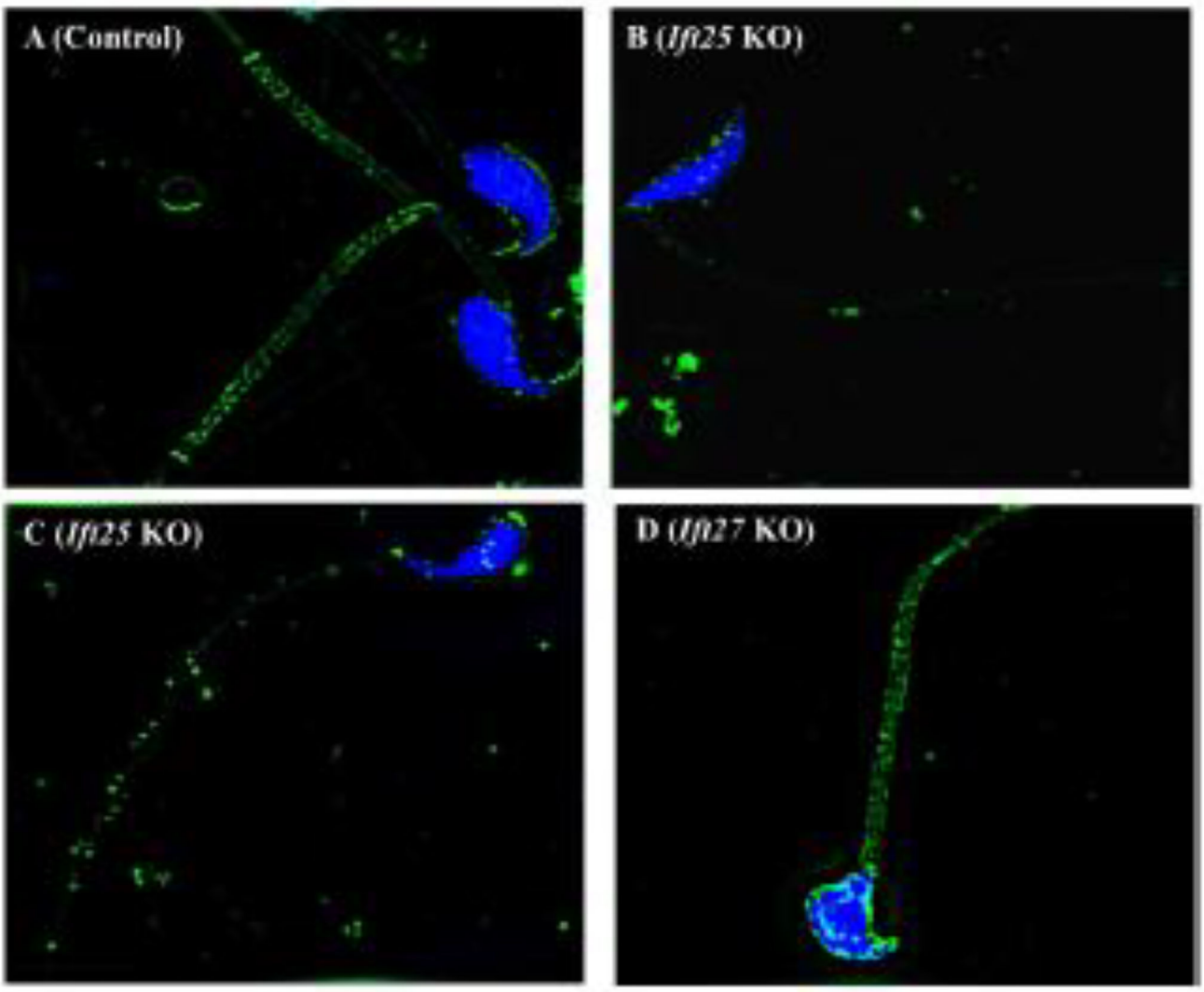

Figure 10. Status of lipid rafts in the control *Ift25* and *Ift27* KO mice

Epididymal sperm were stained with FITC-labeled Cholera Toxin B subunit, and images were captured with a Nikon N-SIM Structured Illumination ("Super-Resolution") Microscope. A. A representative image from a control mouse. Lipid rafts were evenly distributed on the head surface and along the flagella, particularly the middle piece. B and C. Representative images from an *Ift25* KO mouse. In some sperm, lipid rafts were present in the heads, but the signal scattered, and almost no signal was present in the tail (B). Some sperm had almost no signal in the head, but appeared to have scattered signal along the tail (C). D. A representative image from an *Ift27* KO mouse. Even though the sperm morphology was abnormal, lipid raft distribution appeared to be normal.

Table 1

Fertility, fecundity of control and conditional *Ift27* mutant mice

6 weeks old mice			Adult mice		
Genotype	**Fertility**	**Litter size**	**Genotype**	**Fertility**	**Litter size**
Control	10/10	8.2±2.1	Control	10/10	8.4±2.4
Ift27 KO	0/10	0	*Ift27* KO	0/10	0

To test fertility, adult and 6 weeks old males were bred to wild-type females for at least two months. Litter size was recorded for each mating.

Dev Biol. Author manuscript; available in PMC 2017 December 01.